

# Magnetospheric Birefringence Induces Polarization Signatures in Neutron-Star Spectra

R. M. Shannon<sup>\*</sup> and J. S. Heyl<sup>†</sup>

*Department of Physics and Astronomy, University of British Columbia, Vancouver, British Columbia, Canada, V6T 1Z1*

Accepted 2006 February 16. Received 2006 February 15; in original form 2006 January 19

## ABSTRACT

We study the propagation of polarization light through the magnetosphere of neutron stars. At intermediate frequencies (the optical through the infrared), both the birefringence induced by the plasma and by quantum electrodynamics influence the observation polarization of radiation from the surface of the neutron star. Because these two processes compete in this regime, we find that polarization observations can constrain the properties of the neutron-star magnetosphere, specifically the total charge density. We calculate both the phase-resolved and the phase-averaged polarization signatures induced by magnetospheric birefringence.

**Key words:** stars : neutron – magnetic fields – radiation mechanisms : general

## 1 INTRODUCTION

The propagation of polarized radio waves away from neutron stars (NSs) has been well understood for many years (Barnard 1986). At this energy scale, it is reasonable to neglect the coupling of the light to vacuum-based QED effects. Lai and Ho (2003ab) have discussed the mechanisms by which polarized X-rays are affected by the atmospheres of NSs. X-ray photons couple the greatest in the atmosphere as the plasma densities and field strengths are sufficiently high. Lai and Ho included vacuum-based effects in their analysis. Similar effects exist at IR/optical wavelengths when propagation of the waves through the magnetosphere (possessing a lower-density plasma and lower strength magnetic field) is considered. This paper presents a model and results that show that there is a wavelength-dependent polarization signature in the IR/optical wavelength as a result of interactions between radiation and the magnetosphere.

For most radio pulsars emission from the magnetosphere itself rather than the surface is thought to dominate the optical and near infrared emission. However, several radio pulsars exhibit optical radiation from the surface (*e.g.* PSR B0656+14, PSR B0950+08 and Geminga) (*e.g.* Zharikov et al. 2004). Radio pulsars are not the only members of the neutron-star menagerie. The optical and near-infrared emission from the radio quiet neutron stars such as RX J1856.5-3754 and RX J0720.4-3125 (*e.g.* Pons et al. 2002; Motch et al. 2003) most likely comes from the sur-

face, and possibly the emission from anomalous x-ray pulsars emerges from a surface layer heated by magnetospheric currents (Thompson & Beloborodov 2004). With these objects in mind let us proceed.

To make progress we will make several simplifying assumptions. First, we assume that the charge carriers both positive and negative have the mass of an electron and that the plasma is cold. A pair plasma is necessarily hot. Second, we assume that the Goldreich-Julian model is correct. The Goldreich-Julian picture describes the equilibrium charge density for a rotating neutron star with its magnetic pole aligned (or anti-aligned) with the spin axis. Here we will assume that the two axes are not necessarily aligned (especially in § 3.2). Finally, the Goldreich-Julian equilibrium even in its realm of applicability is unstable (see Michel 2004). In spite of these deficiencies, the Goldreich-Julian model provides a well-understood starting point to demonstrate that observations of polarization of the surface radiation from neutron stars may provide a window to diagnose the properties of the plasma and to encourage further research to probe more realistic models.

## 2 CALCULATIONS : POLARIZATION EVOLUTION

Kubo & Nagata (1983) outline how the polarization of light is affected by a birefringent and dichroic medium:

$$\frac{d\vec{s}}{dz} = \hat{\Omega} \times \vec{s} + (\hat{T} \times \vec{s}) \times \vec{s}. \quad (1)$$

This equation is valid for a medium with dispersion, emission and absorption but not scattering. The polarization is described in terms of normalized Stokes parameters  $\vec{s} =$

<sup>\*</sup> Current Address: Department of Astronomy, Cornell University, Ithaca, New York, United States, 14853; email: ryans@astro.cornell.edu

<sup>†</sup> email: hey1@phas.ubc.ca; Canada Research Chair

$(s_1, s_2, s_3) = (Q/I, U/I, V/I)$ . The vectors  $\hat{\Omega}$  and  $\hat{T}$  are the birefringent and dichroic vectors. We have extended the expressions of Heyl & Shaviv (2000) for a permeable medium to include the effects of the plasma:

$$\hat{\Omega} = \frac{\omega}{2c\sqrt{\epsilon_0}} \begin{pmatrix} (\eta_E \epsilon_B - \epsilon_E \eta_B) \sin^2 \theta \cos 2\phi \\ -(\eta_E \epsilon_B - \epsilon_E \eta_B) \sin^2 \theta \sin 2\phi \\ g \cos \theta (\epsilon_B + \frac{1}{2}(\eta_B - \epsilon_B) \sin^2 \theta) \end{pmatrix}, \quad (2)$$

where  $\omega$  is the angular frequency of the radiation;  $\theta$  is the angle between the direction of propagation and the magnetic field; and  $\phi$  is the angle between the projection of the magnetic field onto the plane perpendicular to the direction of propagation, and the component of the magnetic field in the direction of the magnetic moment of the NS.  $\eta_B$  and  $\epsilon_B$  are components of the permeability tensor, and  $\eta_E$  and  $\epsilon_E$  are components of the dielectric tensor, which are, to first order in the fine-structure constant ( $\alpha_f$ ):

$$\eta_B = 1 + \frac{2}{15} \frac{\alpha_f}{\pi} \left( \frac{B}{B_Q} \right)^2, \quad (3)$$

$$\epsilon_B = 1 + \frac{2}{45} \frac{\alpha_f}{\pi} \left( \frac{B}{B_Q} \right)^2, \quad (4)$$

$$\eta_E = 1 - v + \frac{1}{9} \frac{\alpha_f}{\pi} \left( \frac{B}{B_Q} \right)^2, \quad (5)$$

$$\epsilon_E = 1 - \frac{v}{1-u} - \frac{2}{45} \frac{\alpha_f}{\pi} \left( \frac{B}{B_Q} \right)^2, \quad (6)$$

$$g = \frac{v\sqrt{u}}{1-u}, \quad (7)$$

$$\epsilon_0 = \epsilon_E \epsilon_B \cos^2 \theta + \frac{1}{2} \sin^2 \theta (\eta_E \epsilon_B + \epsilon_B \eta_B) \quad (8)$$

for  $B \ll B_Q$  and  $\hbar\omega \ll m_e c^2$  where  $v = \omega_p^2/\omega^2$ , and  $u = \omega_c^2/\omega^2$ .  $\omega_c = eB/(m_e c)$  is the cyclotron frequency and

$$\omega_p = \sqrt{\frac{4\pi e^2 n_e}{m_e}} = \sqrt{2\Omega\omega_c |\cos \theta'|} \quad (9)$$

is the plasma frequency under the assumptions mentioned in the introduction.

To get the second equality we have assumed the Goldreich-Julian (1969) plasma density,  $n_{GJ} = (\Omega B \cos \theta')/(2\pi e c)$ .  $\Omega = 2\pi/P$  is the spin frequency of the star and  $\theta'$  is the angle between the rotation axis and the local magnetic field.  $B$  is the strength of the magnetic field *perpendicular to propagation direction* and  $B_Q \approx 4.4 \times 10^{13}$  G is the critical QED field. In the range of NSs modeled, it was found that the dichroic vector had little effect on the polarization, and was neglected for subsequent results presented here.

A fourth-order Runge-Kutta integrator with variable step size was used to determine the evolution of the polarization vector from the surface of the star to the light cylinder, along a Schwarzschild null geodesic. The polarization vector  $\vec{s}$  was initially set to be in the direction of the plasma-dominated birefringent vector, as the initial polarization modes are determined by the plasma-rich atmosphere of the NS.

We set the initial conditions by specifying the inclination angle  $\alpha$  (not to be confused with the fine structure constant  $\alpha_f$ ) between the optical axis and the magnetic axis, and the angle  $\beta$  between the plane containing the optical and magnetic axes and the plane containing the photon trajectory. For all the calculations stellar radii  $R = 10^6$  cm

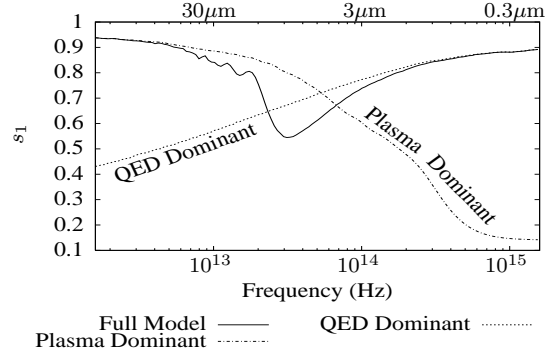


**Figure 1.** Comparison of the three regimes for a neutron star with a one-second spin period and a magnetic dipole moment of  $10^{31}$  G cm<sup>3</sup>, pointing in a direction 60° from the line of sight. The solid line represents the model containing both QED and plasma-based effects, the dot-dashed line shows integrations conducted using only plasma effects, and the short-dashed lines represents integrations conducted with only vacuum-based effects.

and mass  $M = 1.4 M_\odot$  were considered. In addition, we assumed that the NS's magnetic field was dipolar. The output of single integration is similar to Figure 3 of Heyl et al. (2003). The  $s_1$  and  $s_2$  polarizations change considerably as the photon travels away from the NS. At approximately 30 stellar radii, the polarization decouples. The significance of the decoupling radius is discussed below.

### 3 RESULTS

#### 3.1 Net Polarization

The net polarization of the radiation emitted from the NS was determined by integrating over many trajectories on the neutron star image. We sampled the image using regions of equal solid angle using concentric rings about the centre of the NS image. This sampling method could be performed due to the inherent symmetry in the circular NS image. By symmetry, the  $s_2$  and  $s_3$  components of the polarization are zero. Figure 1 shows the frequency-dependent polarization signature for a NS with a dipole moment of  $\mu = 10^{31}$  G cm<sup>3</sup>. The full-model polarization (solid line) is plasma dominated at low frequencies and vacuum (QED) dominated at higher frequencies. In the transitory region, the total polarization suffers some destructive interference between the two processes – the total polarization is less than either the vacuum or plasma-dominated cases.

The location of the minimum in the transitory region can be understood to be the frequency at which the photon decouples from the plasma and vacuum effects at the same time. Using the adiabatic condition, Heyl & Shaviv (2000) determined the criteria for decoupling,

$$\left| \hat{\Omega} \left( \frac{1}{|\hat{\Omega}|} \frac{\partial |\hat{\Omega}|}{\partial r} \right)^{-1} \right| \approx 0.5 \quad (10)$$

Using this expression, the distance at which decoupling occurs can be solved for in both plasma-dominant and QED-dominant regimes. To first order these expressions are:

$$r_{\text{pl, qed}} \propto \mu^{\frac{2}{5}} \omega^{\frac{1}{5}} \times f(\alpha); \quad r_{\text{pl, plas}} \propto \left( \frac{\mu}{P\omega} \right)^{\frac{1}{2}} \times g(\alpha) \quad (11)$$

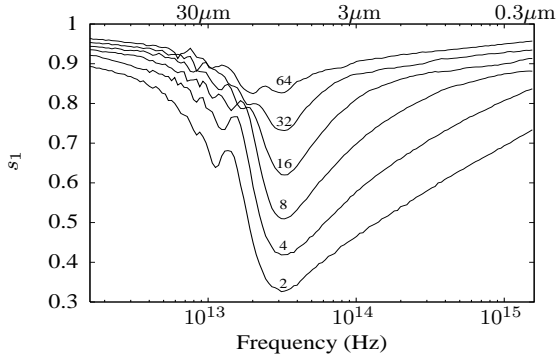


**Figure 2.** Polarization signatures for various magnetic field strengths, with period of 1.0s. The plot shows polarization signatures for increasing magnetic fields, with the lowest line showing a field with a dipole moment of  $2 \times 10^{31} \text{ G cm}^3$ , each subsequent line representing a factor of two increase in the magnetic field to the last line, which shows the polarization signature for a magnetic dipole moment of  $6.4 \times 10^{32} \text{ G cm}^3$ . Above each curve is the magnetic dipole moment in units of  $10^{31} \text{ G cm}^3$ . In each case the dipole points  $30^\circ$  from the line of sight.

Here  $f(\alpha)$  and  $g(\alpha)$  denote the functional dependence of the expressions on the inclination of the star. As the resonance occurs when the photon decouples from both the vacuum and plasma dominated effects at the same time, the critical frequency  $\omega_c$  and the critical radius  $r_c$  at which this resonance occurs are easily calculated:

$$\omega_c \propto \frac{\mu^{\frac{1}{7}}}{P^{\frac{3}{7}}} \times h(\alpha); r_c \propto \frac{\mu^{\frac{3}{7}}}{P^{\frac{3}{7}}} \times j(\alpha) \quad (12)$$

The results of the numerical model were found to be in agreement with these relations.

The critical polarization  $P_c$  (the polarization at resonance) is related to the radius at which photons decouple:  $1 - P_c \propto (R/r_c)^\gamma$  where  $0 < \gamma \lesssim 2$ .

Figure 2 shows how the polarization signature changes as the magnetic field strength is varied. It is observed that as the magnetic field strength is increased, the strength of the resonance feature decreases, but the critical frequency doesn't change significantly. Varying the rotational period of the NS does change the polarization signature. The variation is due to the effects of increased plasma density in the magnetosphere. The results seen in Figure 3 show that as the rotational period is changed the frequency of the dominant features are changed, but the overall structure of the signature remains similar.

It is possible that the charge density of the plasma has been underestimated. Goldreich & Julian (1969) estimate only the net charge density. However, it is possible that the total charge density is larger, as electron-positron pairs may exist in the magnetosphere. Extending the equations of Mézáros (1992) into the formalism presented here, the total charge density can be increased arbitrarily. Figure 3 shows that the introduction of additional charge shifts the resonance to higher frequencies, and decreases the depth of the feature. Again, the overall shape of the feature remains similar. Note that increasing the charge density is comparable to increasing the rotational rate of the NS. At these frequencies increasing the total charge density is nearly covariant with increasing the spin rate of the star, but the ellipticity of the modes depends only on the net charge den-

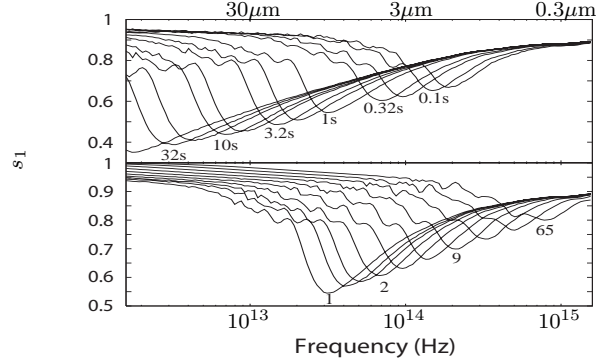


**Figure 3.** Polarization signatures for a dipole moment of  $10^{31} \text{ G cm}^3$  and various periods. The upper panel shows the polarization signatures for various NS periods. The lines show, starting from the most significant minimum on the left periods of 70s, 32s, 20s, 10s, 7s, 3.2s, 2s, 1s, 0.32s, 0.2s, 0.1s, and 0.07s. Some of the minima are labeled with the period. The lower panel gives the results for various total charge densities. The lowest line shows the case in which the total charge density is equal to the net charge density. Each successive line above represents an introduction of an additional component of the total charge density proportional to the net charge density. The second lowest line represents an 25% excess of charge, and each line above that increases the excess by a factor of two. The minima are labeled with the ratio of the total charge to the net charge. In each case the dipole points  $60^\circ$  from the line of sight.

sity so the results for higher net charge density (increasing  $\Omega$ ) and higher total charge density are slightly different.

### 3.2 Phase Integrations

It is currently impractical to measure the instantaneous polarization of an object as faint as a neutron star; therefore it is important to calculate the polarization signature from NS averaged over many spin periods. To do this the polarization must be calculated in a single basis. Heyl et al. (2003) show how the polarization can be calculated. Define the latitude of the optical axis (observer) above rotational equator is as  $i_R$  and the angle between the magnetic axis and rotational axis as  $\gamma$ . If the observer's polarimeter is aligned so that  $s_{O,1}$  is along the rotational equator of the NS and  $s_{O,2}$  is defined  $45^\circ$  to it, the components of the polarization can be determined from the calculations in the other bases<sup>14</sup>

$$s_{O,1} = s_1 \frac{2(\sin \gamma \sin \phi)^2}{1 - (\cos \gamma \sin i_R + \cos i_R \sin \gamma \cos \phi)^2} - 1 \quad (13)$$

$$s_{O,2} = s_1 \frac{2 \sin \gamma \sin \phi (\cos \gamma \cos i_R - \cos \phi \sin \gamma \sin i_R)}{1 - (\cos \gamma \sin i_R + \cos i_R \sin \gamma \cos \phi)^2} \quad (14)$$

The angle  $\alpha$  as defined in the previous section can be calculated using the law of cosines. Figure 4 shows how the polarization from a star evolves as the phase varies. The quadrature sum of the two terms adds to make  $s_{\text{tot}}$ , as expected.

The phase-averaged polarization can be found by computing the mean values in  $s_{O,1}$  and  $s_{O,2}$  with the average

<sup>14</sup> The expression for  $s_{O,2}$  in Heyl et al. (2003) is incorrect by a factor of  $\sin i_R$ . Note that the quadrature sum of  $s_{O,1}$  and  $s_{O,2}$  should be unity. This result is corrected here.

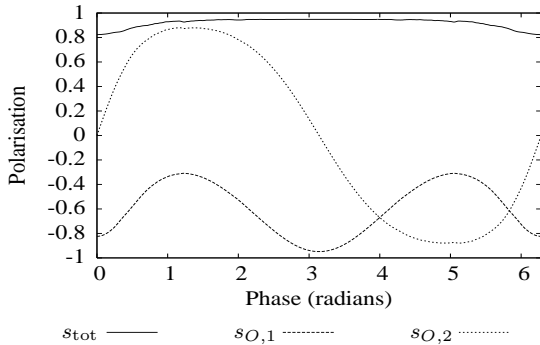


**Figure 4.** Polarization from Neutron Star as a function of phase for a NS with  $\gamma = 30^\circ$  and  $i_R = 30^\circ$ , for  $\omega = 10^{13}$  rad/s and  $\mu = 10^{31}$  G cm<sup>3</sup>.  $s_{\text{tot}}$  is the total polarization at the particular phase.  $s_{O,1}$  is the component of polarization measured in direction perpendicular and parallel to the rotational equator of the NS, and  $s_{O,2}$  is the component  $45^\circ$  to the equator.

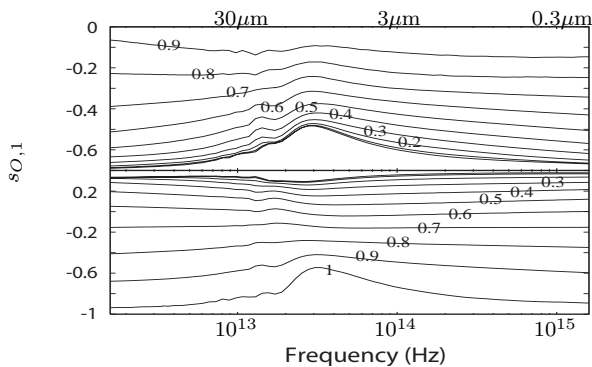


**Figure 5.** Phase-integrated polarization signatures. The upper panel shows polarization signatures for various  $i_R$  with  $\gamma = 30^\circ$ . The lines show how the signature changes from  $\sin i_R = 0$  (bottom line) to  $\sin i_R = 1.0$  (top line, indistinguishable from the x-axis) with each above representing an increase in  $\sin i_R$  of 0.1. The curves are labelled with the value of  $\sin i_R$ . The lower panel shows the results for various  $\gamma$  with  $i_R = 30^\circ$ . The lines show how the signature changes from  $\cos \gamma = 1.0$  (bottom line) to  $\cos \gamma = 0$  (top line) with each above representing a decrement in  $\cos \gamma$  of 0.1. The curves are labelled with the value of  $\cos \gamma$ . In both panels a dipole moment of  $10^{31}$  G cm<sup>3</sup> and an NS period of 1.0s were assumed.

value of  $s_{O,2}$  being zero by symmetry. The lower panel of Figure 5 shows how the signature changes as  $i_R$  varies. Observe that when  $\sin i_R = 1$  (top line) – the observer is looking directly down on the rotation axis – there is no observed polarization. However, for observations at lower latitudes there is a significant net polarization and a resonant feature at approximately  $3 \times 10^{13}$  Hz. Statistically, half of all NS will have inclination angles such that  $\sin i_R \leq 0.5$ . All the models presented in this range show strong features in this range considered.

The upper panel of Figure 5 shows how the signature changes as  $\gamma$  varies. The strongest resonant feature occurs when the magnetic and rotational axes are aligned ( $\gamma = 0$ ). However, strong resonant features can be observed for  $\cos \gamma \geq 0.5$ .

## 4 DISCUSSION

Of particular attention is the wavelength at which the resonant feature occurs – the near infrared. As this energy, it would be possible to measure the polarization of the thermal radiation from a NS using a large ground-based telescope or Hubble’s NICMOS instrument. This instrument is only sensitive to wavelengths less than  $2.1 \mu\text{m}$ , so it is possible that a large portion of the behaviour could not be probed. If the total plasma density is significantly larger than the Goldreich-Julian plasma density, the feature moves into near infrared or optical energies, and more observing options become available.

This letter presents a model for the evolution of polarized light through the magnetosphere of highly magnetized neutron stars. We found that the polarization has a frequency-dependent signature, where the total polarization decreases significantly in the optical or near IR, dependent on the plasma density near the neutron star and the structure of the magnetic field. Observations of neutron stars in this frequency region may provide useful probes of the properties of neutron-star magnetospheres and elucidate the processes responsible for pulsar emission.

## ACKNOWLEDGMENTS

The Natural Sciences and Engineering Research Council of Canada supported this work. Correspondence and requests for materials should be addressed to J.S.H.([hey1@phas.ubc.ca](mailto:hey1@phas.ubc.ca)).

## REFERENCES

- Barnard J. J., 1986, ApJ, 303, 280
- Goldreich P., Julian W., 1969, Ap. J., 157
- Heyl J., Shaviv N., 2000, MNRAS, 311
- Heyl J. S., Shaviv N. J., Lloyd D., 2003, MNRAS, 342
- Kubo H., Nagata R., 1983, J. Opt. Soc. Am., 73
- Lai D., Ho W., 2003a, Phys. Rev. Lett., 91, 071101
- Lai D., Ho W., 2003b, Ap. J., 588, 962
- Mézáros P., 1992, High Energy Radiation From Neutron Star Magnetospheres. University of Chicago, Chicago
- Michel F. C., 2004, Advances in Space Research, 33, 542
- Motch C., Zavlin V. E., Haberl F., 2003, Astron. Astrophys., 408, 323
- Pons J. A., Walter F. M., Lattimer J. M., Prakash M., Neuhäuser R., An P., 2002, Astrophys. J, 564, 981
- Thompson C., Beloborodov A. M., 2004, ArXiv Astrophysics e-prints
- Zharikov S. V., Shibanov Y. A., Mennickent R. E., Komarova V. N., Koptsevich A. B., Tovmassian G. H., 2004, Astron. Astrophys., 417, 1017